Pet. Sci. (2016) 13:402–417
DOI 10.1007/s12182-016-0110-9

ORIGINAL PAPER

Selective dissolution of eodiagenesis cements and its impact on the quality evolution of reservoirs in the Xing'anling Group, Suderte Oil Field, Hailar Basin, China

Zhen-Zhen Jia[1,2] · Cheng-Yan Lin[1,2] · Li-Hua Ren[1,2] · Chun-Mei Dong[1,2]

Received: 28 February 2015 / Published online: 30 July 2016

Abstract Reservoirs in the Xing'anling Group in the Suderte Oil Field, Hailar Basin exhibit ultra-low to low permeability and high tuffaceous material content. This study comprehensively analyzed diagenesis and quality evolution of these low-permeability reservoirs using thin sections, SEM samples, rock physical properties, pore water data, as well as geochemical numerical simulations. Calcite and analcite are the two main types of cements precipitated in the eodiagenetic stage at shallow burial depths in the reservoirs. These two cements occupied significant primary intergranular pores and effectively retarded deep burial compaction. Petrography textures suggest selective dissolution of massive analcite and little dissolution of calcite in the mesodiagenetic stage. Chemical calculations utilizing the Geochemist's Workbench 9.0 indicated that the equilibrium constant of the calcite leaching reaction is significantly smaller than that of the analcite leaching reaction, resulting in extensive dissolution of analcite rather than calcite in the geochemical system with both minerals present. Numerical simulations with constraints of kinetics and pore water chemistry demonstrated that the pore water in the Xing'anling group is saturated with respect to calcite, but undersaturated with analcite, leading to dissolution of large amounts of analcite and no dissolution of calcite. Significant secondary intergranular pores have formed in analcite-cemented reservoirs from selective dissolution of analcite in the mesodiagenetic stage; the analcite dissolution formed preferential flow paths in the reservoirs, which promoted feldspar dissolution; and dissolution of such minerals led to the present reservoirs with medium porosity and low permeability. Calcite-cemented tight reservoirs have not experienced extensive dissolution of cements, so they exhibit ultra-low porosity and permeability.

Keywords Eodiagenetic cements · Calcite · Analcite · Selective dissolution · Secondary porosity · Hailar Basin

1 Introduction

Early cementation (e.g., carbonate cementation, zeolite cementation) in clastic reservoirs has considerable impact on reservoir quality evolution, as it may slow subsequent burial compaction and provides significant potential minerals for burial dissolution (Yuan et al. 2015a; Dutton and Loucks 2010; Fu et al. 2010; Yu and Lai 2006; Schmidt and McDonald 1979; Zhu et al. 2012). Recent studies have suggested that early zeolite cements (e.g., analcite, laumontite) can be dissolved extensively at the mesodiagenetic stage to form secondary pores, enhancing reservoir porosity and permeability (Tang et al. 1997; Zhu 1985; Meng et al. 2013; Sun et al. 2014; Zhu et al. 2011). However, there is significant disagreement among various authors regarding burial dissolution of carbonate cements in clastic reservoirs. In broad terms, there are two major schools of thought (Bjørlykke and Jahren 2012; Giles 1987; Giles and Marshall 1986; Yuan et al. 2015a, b). One group of authors considers that carbonate cements can be leached during burial to generate significant secondary porosity and improve reservoir quality (Schmidt and McDonald 1979;

✉ Cheng-Yan Lin
ycdzycms@126.com

[1] School of Geosciences, China University of Petroleum, Qingdao 266580, Shandong, China

[2] Key Laboratory of Reservoir Geology in Shandong Province, Qingdao 266580, Shandong, China

Edited by Jie Hao

Zhong et al. 2003; Yu and Lai 2006). The other group of authors suggests that carbonate cement cannot be dissolved extensively at the deep burial stage, but that carbonate cementation degrades reservoir porosity and permeability (Bjørlykke and Jahren 2012; Giles and Marshall 1986; Taylor et al. 2010; Yuan et al. 2013, 2015a, b, c; Shou 2005). The reservoirs in the Xing'anling Group in the Suderte Oilfield of the Hailar Basin, which are characterized by abundant volcanic materials, are mostly low to ultra-low permeability reservoirs (Wang et al. 2012). Calcite and analcite are two main types of early cements in these reservoirs, and thin sections and SEM samples demonstrate extensive selective dissolution of analcite cement. However, there is not much evidence supporting the dissolution of associated calcite cement in the Xing'anling Group. Reservoirs with extensive dissolution of analcite are characterized by significant secondary pores, and the core porosity of such reservoirs can reach up to 20 %–25 %, while the core porosity of poor-quality reservoirs with massive calcite cement is generally lower than 10 %–15 % due to limited burial dissolution. To this effect, understanding the origin and processes at work in the selective dissolution of these two cements benefits reservoir quality prediction (Yuan et al. 2015a).

The selective dissolution phenomena of different minerals in sediments have garnered quite a bit of attention from geologists in recent years (Cao et al. 2014; Macquaker et al. 2014; Turchyn and Depaolo 2011; Yuan et al. 2015a). Macquaker et al. (2014) and Turchyn and Depaolo (2011), for example, reported similar phenomena in fine-grained sediments (Macquaker et al. 2014; Turchyn and Depaolo 2011) and Yuan et al. (2015a) investigated the selective dissolution between feldspars and calcite in buried sandstones. Other geologists have studied genetic mechanisms of the selective dissolution phenomena between zeolites and calcite via static plots, including Gibbs free energy versus temperature (burial depth) profiles (Meng et al. 2013, 2014; Qi 2013; Xiu 2008; Zhao 2005) and equilibrium constant versus temperature profiles (Qi 2013; Zhao 2005) of leaching reactions of different minerals. Studies of water–rock interactions in geochemical systems considering both minerals over extended periods of time and kinetics-related constraints, however, are relatively few. In effort to remedy this, the present study was conducted with the following main objectives: (1) to investigate sandstone diagenesis using cores, thin sections, and SEM sample analysis, (2) to analyze various impacts of selective dissolution of analcite and calcite on reservoir quality evolution by testing physical properties, and (3) to decipher the genetic mechanism of selective dissolution between analcite and calcite using the Geochemist's Workbench (GWB) 9.0 with constraints of pore water chemistry and kinetic data.

2 Geological settings

Suderte Oilfield, with an exploration area of about 200 km^2, is located near the middle of the Suderte tectonic zone in the Beier Sag of the Hailar Basin. The tectonic zone is cut by NE-trend and WE-trend faults, splitting the oilfield into several NEE-trend fault blocks. The sediments in the oilfield contain the Triassic Budate Formation, Cretaceous Tongbomiao, Nantun, Damoguaihe, Yimin, and Qingyuangang Groups, and Cenozoic Formation, from base to top. The Tongbomiao Group and the first member of the Nantun Group have been further divided into six oil group members marked X0–XV (Fig. 1), which constitute the Xing'anling Oil Group, the major oil-bearing sequence in the area. The sedimentary strata in the study area feature large structural altitude differences and significant thickness variations caused by fault impacts. Reservoirs in oil group members XI and XII, which show stable spatial distribution, are the main focus of this study.

During the depositional period of the first member of the Nantun Group, the Suderte tectonic zone was a small rift basin controlled by multiple fault terraces. The steep slope zone of the rift basin was characterized by large altitude differences and, of course, steep slopes. The alluvial fan depositional systems, with mainly southwest and southeast source supplies, entered the lakes quickly to form fan deltas; multisource fan deltas were interconnected to form fan delta aprons distributed along the fault margins (Wang et al. 2012). Studies on zircon U–Pb chronology have demonstrated that volcanic activity in the Hailar Basin continued during the late Jurassic to the early Cretaceous period, with stronger activity in 128–117 and 116–113 Ma (Chen et al. 2015; Zhao et al. 2013). Impacted by simultaneous volcanic eruptions during the depositional period, rocks in the XI–XIV oil group members generally contain volcanic debris (Xiao et al. 2011), consisting mainly of tuff conglomerate, tuff sandstones, and some sedimentary tuff.

Burial and thermal histories of the Suderte tectonic zone show that the Nantun Formation experienced four stages: rapid subsidence, uplift, slow subsidence, and stability (Fig. 2) (Song 2013; Shen et al. 2013). The paleo Formation temperature gradient in the Cretaceous was about 4.2–5.6 °C/100 m, higher than the present temperature gradient (3.30 °C/100 m) (Cui et al. 2011). Burial and thermal histories of well Bei-30 show that the Nantun Formation experienced its deepest burial depth and highest formation temperature by the end of the early Cretaceous, after which formation temperature decreased continually with uplift and decreasing temperature gradient. The present burial depth and temperature are below maximum burial depth and temperature.

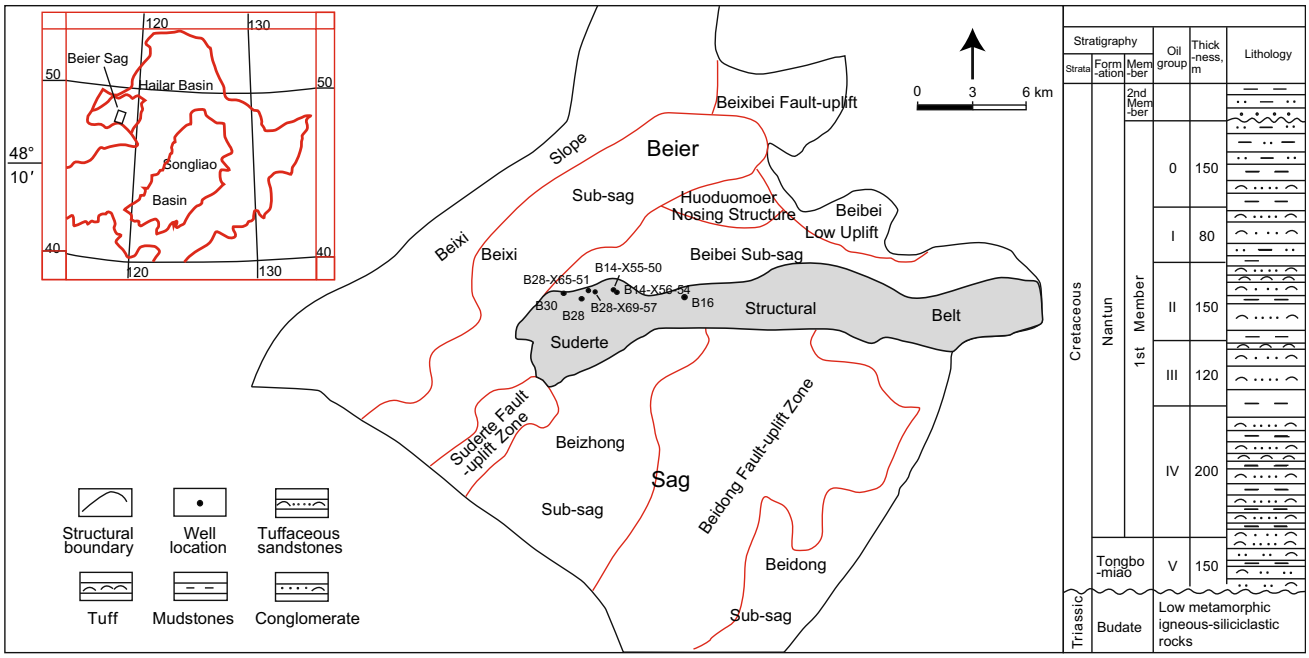

Fig. 1 Location map of the Beier Sag, Hailar Basin, subunits in the Beier Sag, and sedimentary strata in the Suderte Oilfield. Modified from Wang et al. (2012)

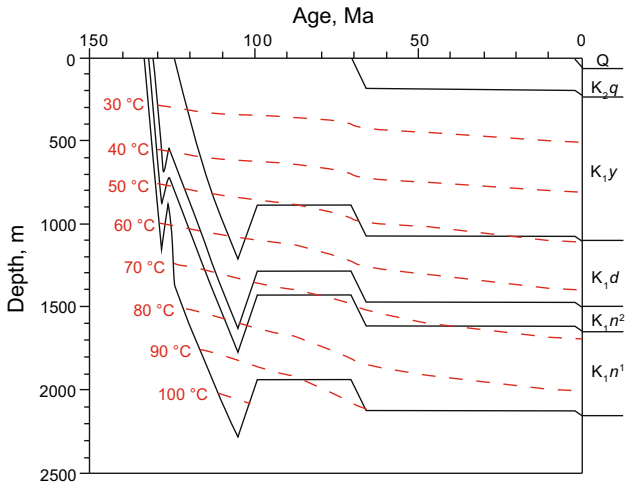

Fig. 2 Burial and thermal history of well Bei-30 in the Suderte Oilfield. Modified from Song (2013)

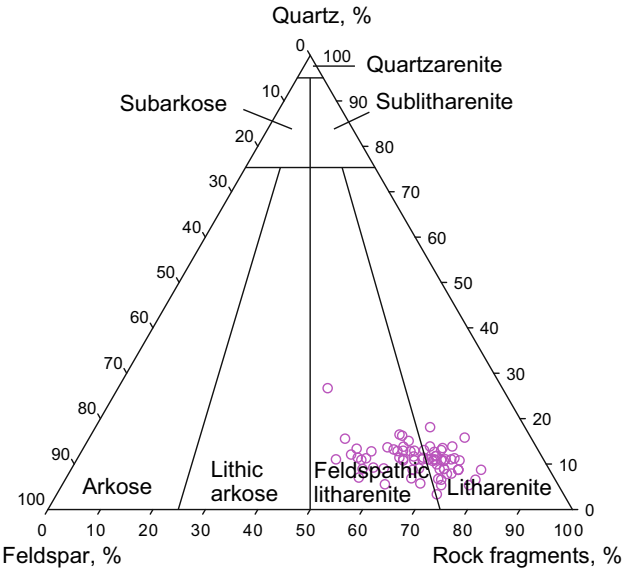

Fig. 3 Ternary plots showing grain composition of sandstones in the Xing'anling Group, Suderte Oilfield

3 Petrography

Members XI–XII in the Xing'anling Group in the Suderte Oilfield are mainly composed of fine sandstones, medium- to coarse-grained sandstones, fine-grained conglomerates, and siltstones, as evidenced by core observation and thin section identification. The siltstone and conglomerates are rich in tuffaceous matrix, and the sandstones are composed of feldspathic litharenite and litharenite (Fig. 3) that are texturally and compositionally immature. The sandstones contain an average of 10 % detrital quartz grains, 20 % feldspar, and 70 % rock fragments which consist mainly of andesitic and rhyolitic tuff (up to 80 %), followed by sedimentary rock fragments. The amount of intergranular fillings ranges from 10 % to 25 %, including 8 %–20 % authigenic cements and less than 5 % matrix (detrital clays and volcanic ash). Authigenic minerals consist mainly of calcite, analcite, and kaolinite. On the whole, detrital grains

are moderately to poorly sorted, detrital rock fragments are present in subangular shapes and detrital quartz grains in subangular or subrounded shapes. Grain contacts are mainly line–line and concavo–convex.

4 Diagenesis

4.1 Types and characteristics of diagenesis

4.1.1 Compaction

Compaction is a major factor affecting porosity and permeability reduction during reservoir burial (Lu et al. 2015; Zhang et al. 2014; Zhu et al. 2010; Xu et al. 2008; Cao et al. 2012, 2014; Pittman and Larese 1991; Xi et al. 2015). Due to their high content of ductile tuff debris, Xing'anling Group rocks have low compaction resistance and are generally strongly compacted (Mousavi and Bryant 2013; Pittman and Larese 1991) (Fig. 4a). The development of early cementation can effectively retard compaction. In sandstones with little cement, detrital grain contacts are mainly line–line and concavo–convex as opposed to point–line. In sandstones with abundant cements, conversely, grain contacts are mainly line–point and point–line. Quantitative statistics show that in reservoirs with high cement (calcite) content, reservoirs exhibit porosity loss from compaction of about 10 %–20 %. In reservoirs with relatively low cement content but well-developed intergranular secondary pores formed during analcite dissolution (analcite cementation occurred in the eodiagenetic stage), porosity loss due to compaction is nearly 20 %–

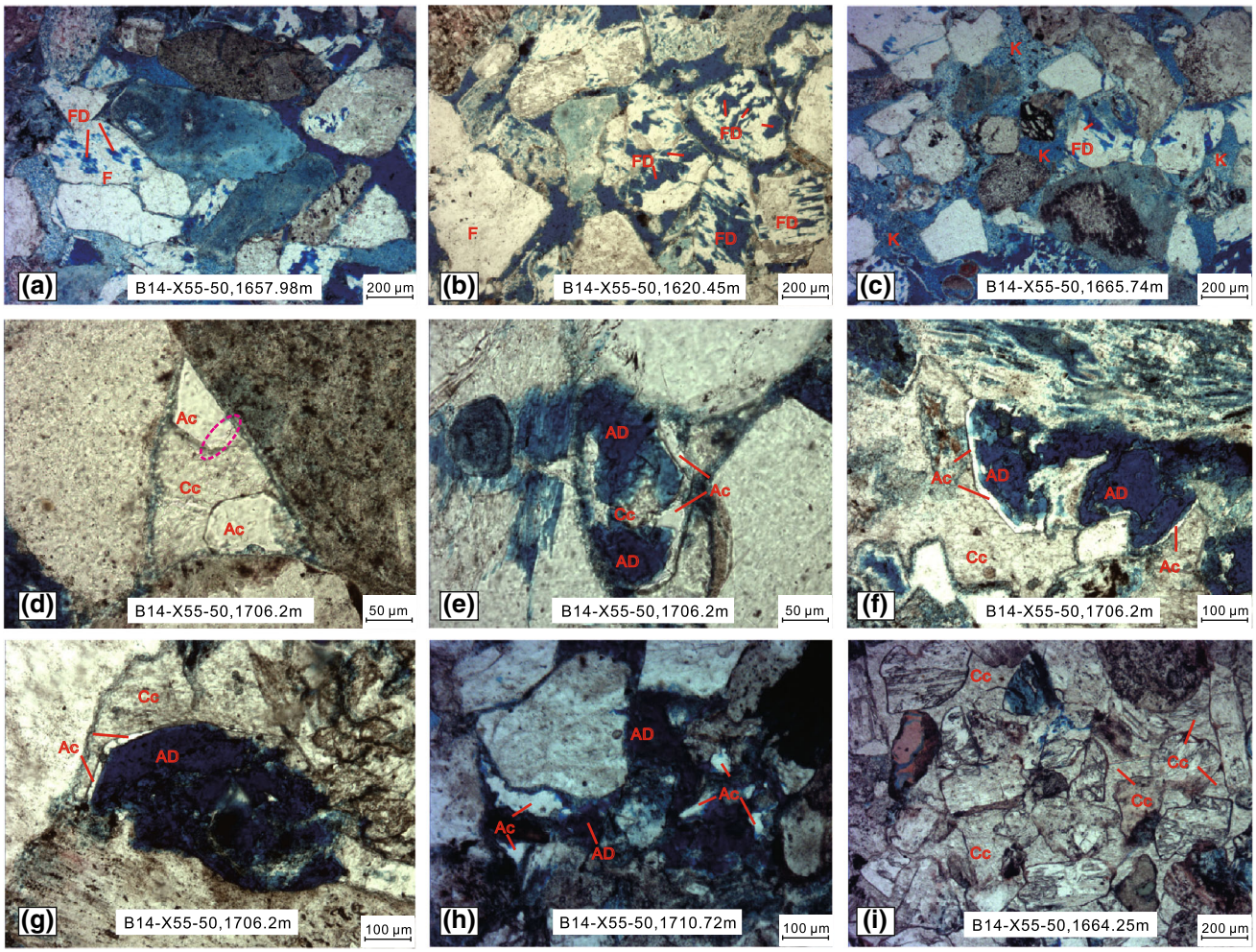

Fig. 4 Microscope photos of thin sections of sandstones in the Xing'anling Group. **a** Mechanical compaction, grains in concavo–convex-linear contact; **b** dissolved feldspars and intergranular secondary pores; **c** dissolved feldspar and authigenic kaolinite; **d** analcite dissolution remnants and early calcite cement, where analcite was partially replaced by calcite; **e** late carbonate cement in secondary pores formed by analcite dissolution; **f**, **g** selective dissolution of analcite in the presence of early calcite cement; **h** analcite remnants after dissolution; **i** tight sandstones cemented by large amounts of early calcite. *FD* secondary pores formed by feldspar dissolution, *K* kaolinite, *Cc* carbonate cement, *Ac* analcite

25 %. While in reservoirs with relatively low-cement content and poorly developed secondary pores (weak cementation occurred in the eodiagenetic stage), porosity loss due to compaction is approximately 30 %–35 %.

4.1.2 Cementation

Cementation also has significant impact on reservoir quality evolution during burial. Various cements in the Xing'anling Group reservoirs include calcite, analcite, kaolinite, and a small amount of quartz.

1. Carbonate cementation.
   Carbonate is the most important cement component in the Xing'anling sandstones. The mineral texture of carbonate cement and the relationship between carbonate cement and secondary pores indicate the existence of abundant stage-I calcite cement (early calcite) and a small amount of stage-II calcite cement (late calcite). In early calcite-cemented tight sandstones, cements occupy almost all primary pores and can account for 25 %–30 % of the total sandstone volume. Generally, early calcite-cemented sandstones are supported by detrital grains with point–point contacts or with floating texture (Fig. 4i), implying there was little compaction when cementation occurred (Gluyas and Coleman 1992; Yuan et al. 2015b, c). The content of late calcite cement is generally less than 1 % and this has only slight impact on reservoir quality. Late calcite cement occurred mainly in secondary pores in the study reservoirs, forming after the dissolution of feldspars and analcite.
2. Analcite cementation.
   The abundance of volcanic materials in the reservoirs of the Xing'anling Group and the early alkaline environment following deposition facilitated cementation of zeolite (Tang et al. 1997; Xiao et al. 2011; Zhu et al. 2011). Textures in thin sections indicate a competitive relationship between analcite and calcite cements (Fig. 4d–g), which plays a key role in controlling reservoir quality evolution. In the reservoirs, this competitive relationship is indicated by the negative relationship between the amount of carbonate cement and the amount of analcite and analcite secondary pores (Fig. 5). The analcite cement was precipitated in the form of pyritohedron single crystals and blocky aggregates in intergranular pores (Fig. 6b), and currently occurs primarily as dissolution remnants (Fig. 4e–h). Petrography texture of the replacement of analcite by calcite (Fig. 4d) indicates that the formation of analcite cement was just prior to or synchronous with that of calcite cement.

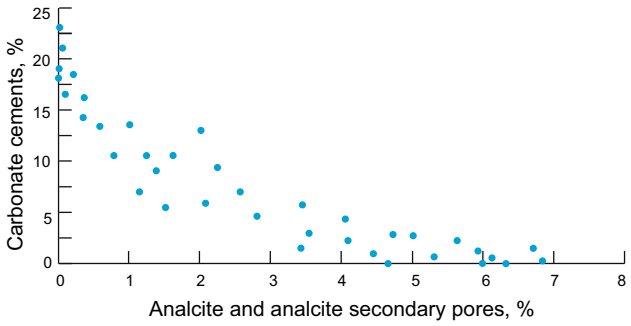

Fig. 5 Negative relationship between the amount of carbonate cement and the amount of analcite and analcite secondary pores in the reservoirs in the Xing'anling Group

3. Authigenic clays.
   Volcanic rock fragments in reservoirs of the Xing'anling Formation consist mainly of acidic andesite and rhyolitic tuff, exhibiting weak dissolution. Some secondary micropores occurred in fragments through partial hydrolysis of these grains. Tuffaceous matrix was abundant in the reservoirs and this has experienced complex diagenesis. In the eodiagenetic stage, the tuffaceous matrix was transformed to chlorite and illite/smectite (I/S) in the presence of alkaline water. Chlorite was precipitated mainly as grain rims (Fig. 4e), which may have retarded quartz cementation in the mesodiagenetic stage. Kaolinite is the most important authigenic clay mineral in the reservoirs, at relative content up to 70 %–80 % of the total clay minerals in the sandstones (Fig. 7). Kaolinite occurs mainly in the sandstones with abundant secondary pores, and is scarce in calcite-cemented, tight rocks. This textural relationship indicates that the precipitation of kaolinite occurred after early carbonate cementation, probably in the mesodiagenetic stage, and as a byproduct of dissolution of feldspars and analcite. Single kaolinite crystals generally show hypidiomorphic pseudohexagonal structure, and the size of kaolinite platelets is usually less than 5–8 μm in width with thickness less than 0.5 μm. Kaolinite aggregates, mainly in short vermiform shape and booklet-like shape, are generally less than 20 μm in length. Kaolinite is distributed in a relatively dispersed pattern in the study area, and contains abundant intercrystal micropores (Figs. 4c, 6c).
4. Quartz cementation.
   Petrography reveals that quartz cementation is relatively weak in the sandstones. Quartz cement occur mainly as small quartz crystals (<5–10 μm) (Fig. 6d), and quartz overgrowth cannot be identified in thin section or SEM samples. The impact of quartz cementation on physical properties of reservoirs is

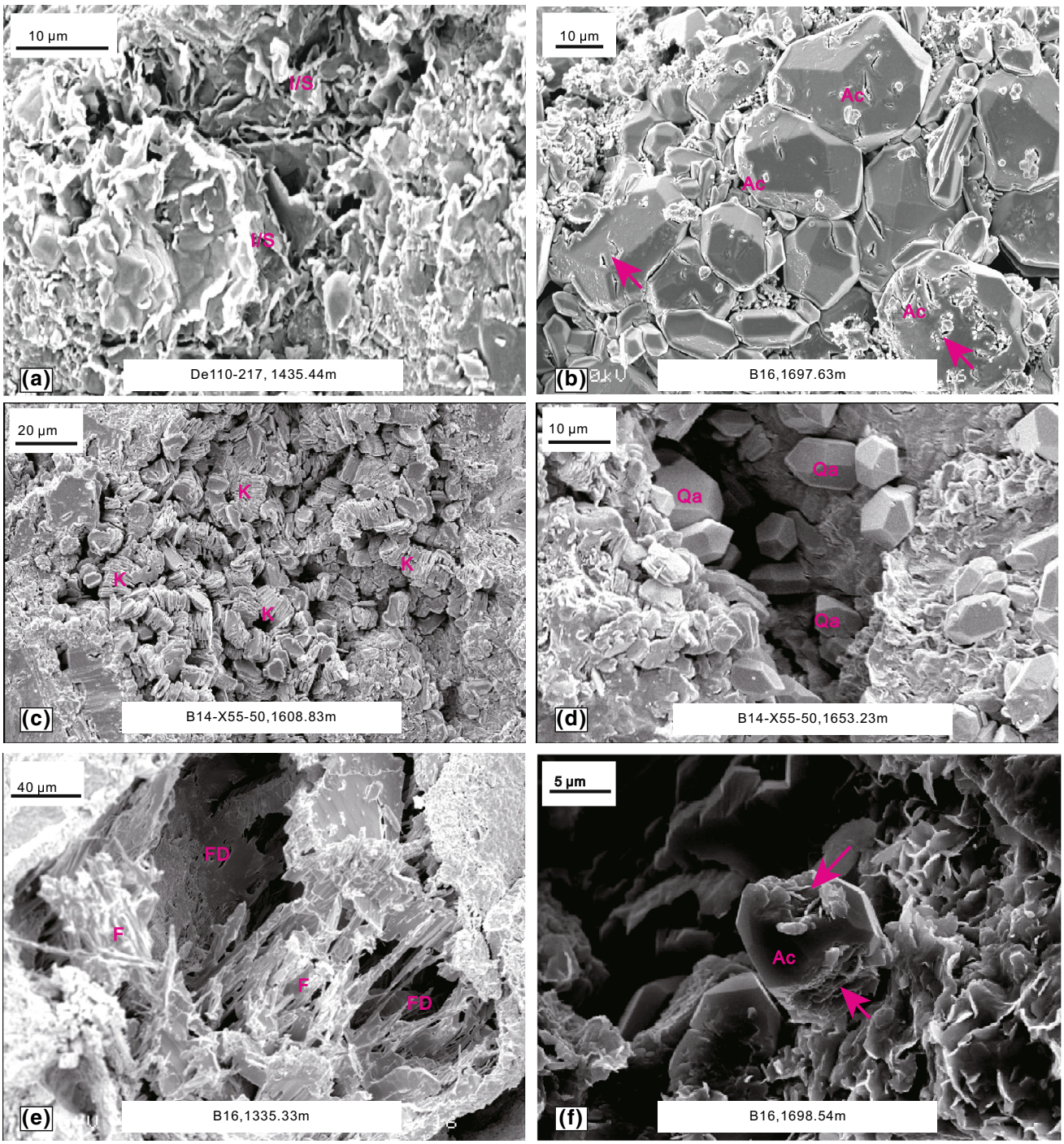

Fig. 6 SEM micrographs of sandstones in the Xing'anling Group, Suderte Oilfield. **a** Mixed layer illite/smectite (I/S) in sandstones; **b** analcite (Ac) in intergranular pores; **c** kaolinite (K) in pores; **d** quartz crystals (Qa) in intergranular pores; **e** extensively dissolved feldspar (F); **f** analcite (Ac) and corroded notches

insignificant. Authigenic quartz occurs mainly in the reservoirs with abundant secondary pores, and is scarce in calcite-cemented tight rocks, indicating that quartz cementation occurred after early carbonate cementation, probably in the mesodiagenetic stage, and also as a byproduct of dissolution of analcite and feldspars.

4.1.3 Selective dissolution of minerals

Mineral dissolution generally improves reservoir quality (Schmidt and McDonald 1979; Surdam et al. 1984; Yuan et al. 2015c; Cao et al. 2012; Zhu et al. 2007; Han et al. 2007). Vitrinite reflectance (R_0 %) of organic matter in

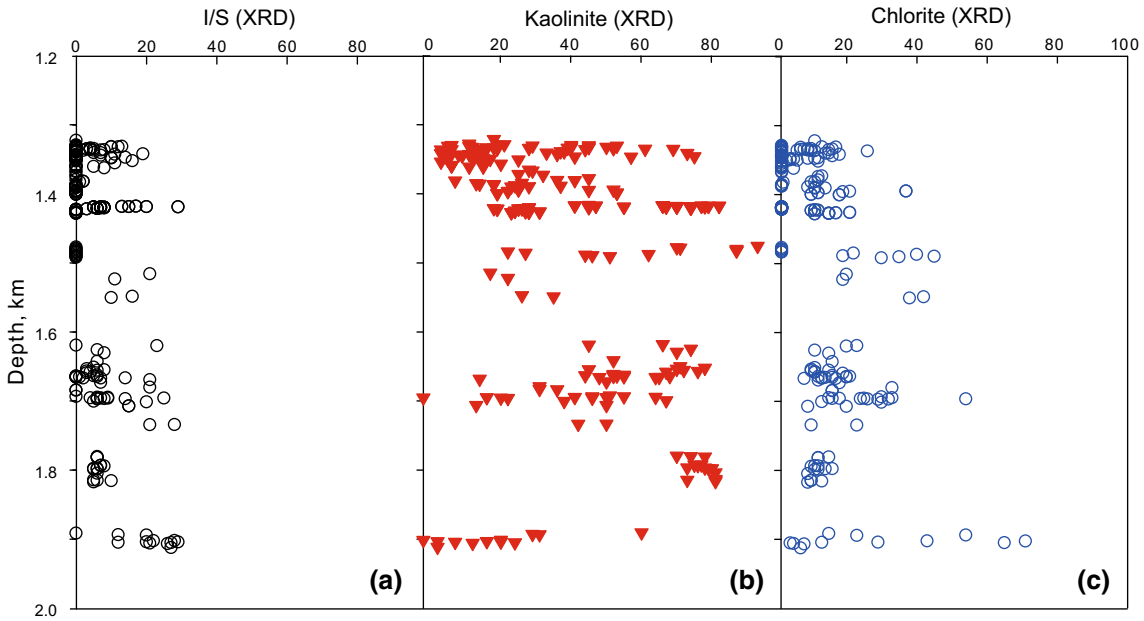

Fig. 7 Relative contents of illite–smectite, kaolinite, and chlorite in sandstones in the Xing'anling Group, Suderte Oilfield

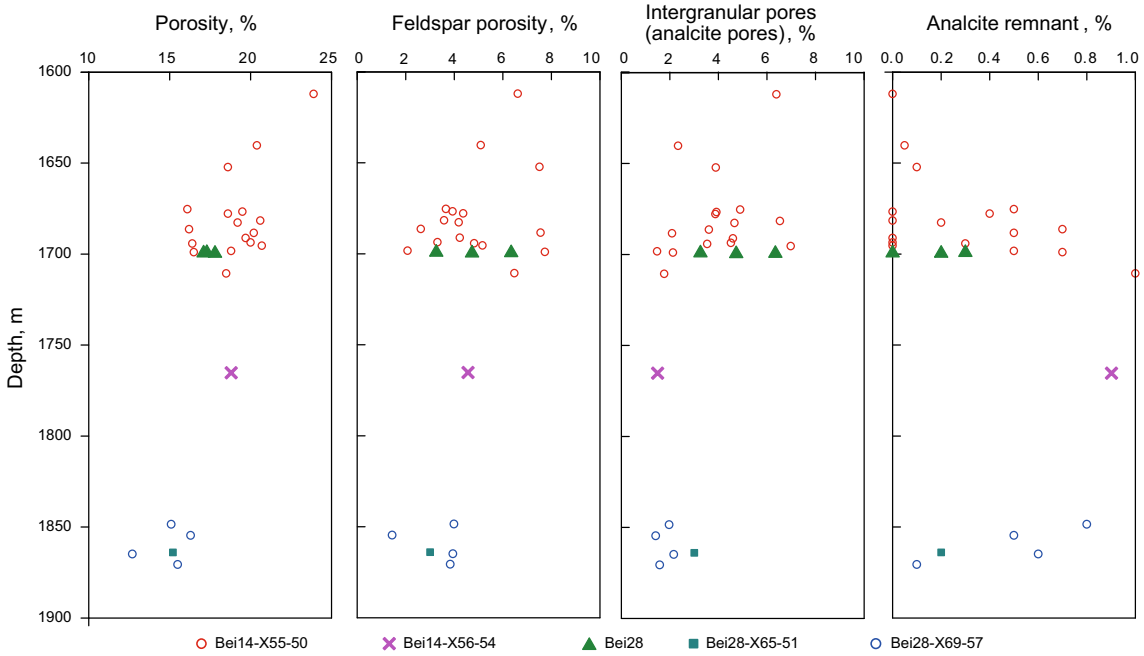

Fig. 8 Plots of porosity, feldspar porosity, intergranular pores (analcite pores), and remnant analcite in high-quality reservoirs in the Xing'anling Formation

interbedded mudstones in the Xing'anling Group is up to 0.8 %–1.0 %, and thermal evolution of such organic matter has produced large amounts of CO_2 and organic acids, which have probably leached unstable minerals (Schmidt and McDonald 1979; Surdam et al. 1984; Yuan et al. 2015a). Petrography textures show that in sandstones with extensive cementation of early calcite, the calcite cement was apparently not leached. As the calcite cement clogged fluid flow paths, feldspar in the sandstones were also not dissolved extensively. In sandstones with weak calcite cementation but extensive analcite cementation, extensive dissolution of analcite and feldspars occurred and formed a large amount of secondary porosity (Figs. 4b, c, 4e–h, 6e, 8). There is no petrographic evidence, however, supporting dissolution of the associated calcite cements in such porous sandstones (Fig. 4d–g). Differing from past studies which

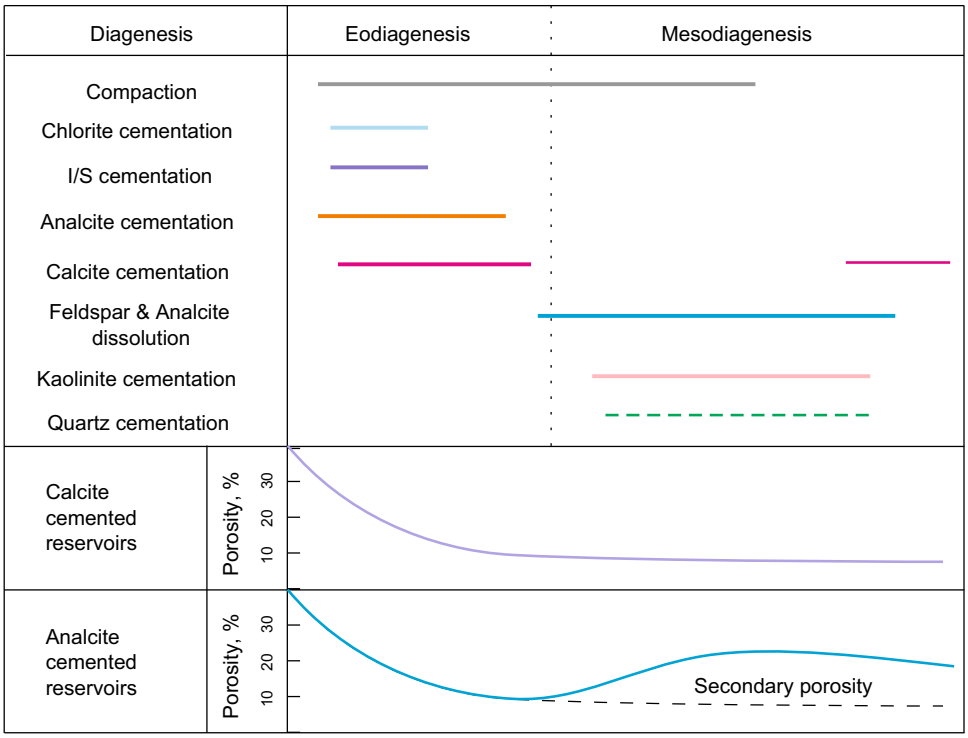

Fig. 9 Diagenetic sequences and porosity evolution model of different reservoirs in the Xing'anling Formation

suggested that carbonate minerals could be easily dissolved by acidic fluids, this selective dissolution of analcite in the presence of calcite in the studied reservoirs is quite interesting (Macquaker et al. 2014; Yuan et al. 2015a).

4.2 Diagenetic sequences

The relative timing of the major diagenetic sequence of the sandstones in the Xing'anling Group, which has been determined from thin sections and SEM examination, is based on texture relationship of cementation, dissolution, and replacement of various minerals (Figs. 4, 6). In summary, the integrated diagenetic sequences consist of compaction/chlorite cementation/early analcite cementation/early calcite cementation–analcite dissolution/feldspar dissolution/authigenic kaolinite precipitation/quartz cementation–late carbonate cementation (Fig. 9).

5 Early cements and reservoir properties

The selective dissolution of early analcite cement and calcite cement at the mesodiagenetic stage led to significant differences in properties among various reservoirs.

5.1 Reservoirs with eodiagenetic cementation and mesodiagenetic nondissolution of calcite

Thin sections and SEM samples demonstrate that in reservoirs with extensive calcite cementation, primary intergranular pores are occupied almost entirely by calcite cement. Reservoir spaces consist of a few residual micropores and secondary pores formed by dissolution of feldspars and analcite, and the content of pores in thin sections is commonly lower than 0.1 %. Physical properties of such sandstones show that the calcite-cemented tight sandstones are typically found in low-porosity and ultra-low permeability reservoirs (Fig. 10a1, b1, c), with porosity lower than 15 % and permeability lower than 0.1 mD. These sandstones are characterized by poor pore structures, generally with micropores and microthroats. High-pressure mercury injection tests matched with thin section examination demonstrate that mercury injection curves are characterized by high initial replacement pressure and low injection saturation. Initial replacement pressure is generally higher than 5 MPa, maximum pore-throat radius is lower than 0.2 μm, average pore-throat radius is lower than 0.05 μm, mercury injection saturation is below 50 %, and mercury withdrawal efficiency is below 30 %.

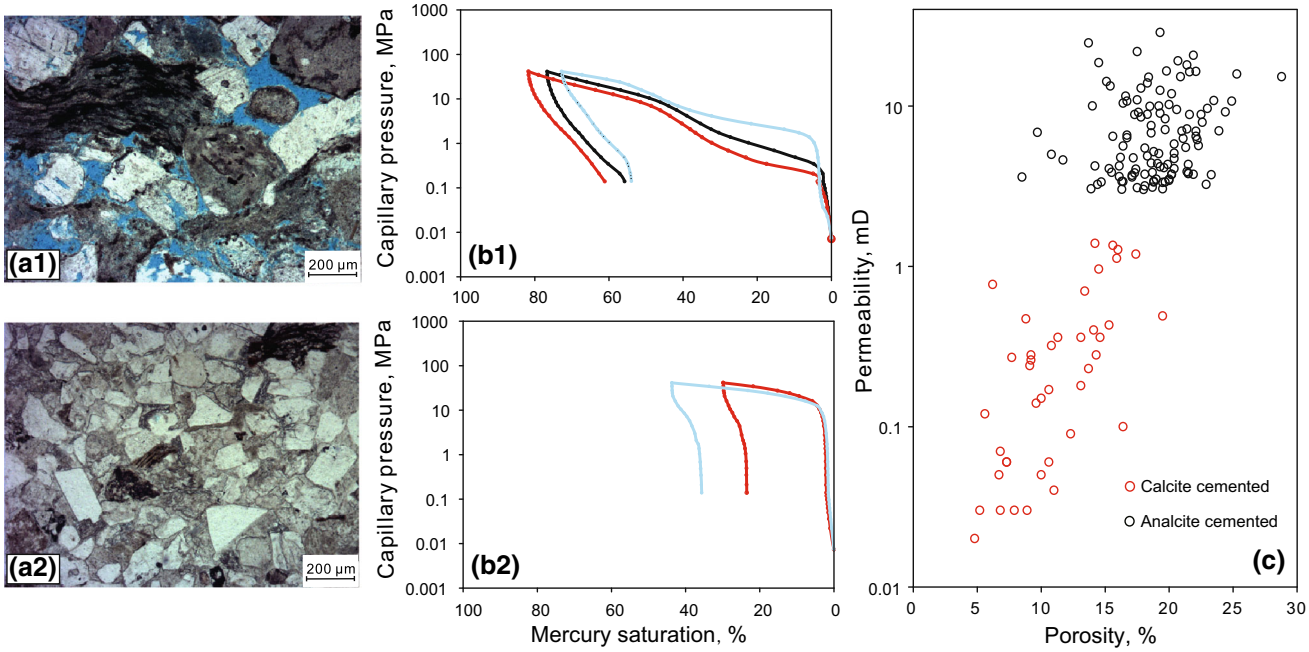

Fig. 10 Comparison of reservoir pores, pore structures, and physical properties of two different types of reservoirs. **a1–b1** Pores and mercury injection curves of reservoirs with extensive analcite dissolution; **a2–b2** pores and mercury injection curves of reservoirs with extensive early calcite cementation; **c** porosity versus permeability plots of the two different types of reservoirs

5.2 Reservoirs with eodiagenetic cementation, mesodiagenetic dissolution of analcite

Thin sections and SEM samples indicate that in reservoirs with strong early cementation and extensive late dissolution of analcite, spaces are mainly secondary pores formed by dissolution of analcite and feldspars while micropores in kaolinite aggregates, and primary pores are undeveloped. Quantitative analysis of different pores in thin sections shows that secondary pores formed by analcite dissolution range from 2 % to 6 % with an average of 4 %, and secondary pores formed by feldspar dissolution range from 2 % to 7 % with an average of 5 %. Physical properties of these sandstones are much more favorable than those of calcite-cemented tight sandstones, with porosity higher than 15 % and permeability higher than 1 mD; these reservoirs typically show medium porosity and low permeability (Fig. 10a2, b2, c), and sandstones are characterized by moderate pore structures with generally moderate pores and fine- to micro-throats. High-pressure mercury injection tests matched with the thin sections demonstrate that mercury injection curves are characterized by low initial replacement pressure and high injection saturation. The initial replacement pressure is generally lower than 0.1–1 MPa, maximum pore-throat radius is lower than 1 μm, and average pore-throat radius is lower than 0.2 μm.

5.3 Evolution models of reservoir physical properties

For reservoirs with extensive carbonate cementation, burial dissolution is especially weak in reservoirs with abundant calcite, and chemical reactions nearly cease after extensive calcite cementation. The porosity of such sandstones decreased significantly due to strong compaction and extensive calcite cementation, and without significant burial dissolution, the reservoirs still show low porosity now (Fig. 9).

For reservoirs with strong analcite cementation, analcite and feldspars were dissolved extensively, and such reservoir experienced a relatively complete diagenetic sequence. The porosity of these sandstones also decreased significantly with intensive compaction and cementation at the eodiagenetic stage. Extensive dissolution of analcite and feldspars at the mesodiagenetic stage, however, formed large-volume secondary pores, and the current porosity recovered to a relatively high level (Fig. 9).

6 Genetic mechanism of selective dissolution reaction

Laboratory experiments indicated that carbonate minerals can be dissolved much faster than aluminosilicate minerals (Arvidson et al. 2003; Yuan et al. 2015a). However, recent

studies suggested that feldspars can be selectively dissolved in the presence of carbonate minerals in buried sandstones (Yuan et al. 2015a). The selective dissolution of analcite in the presence of calcite is also interesting as a departure from the results of traditional laboratory experiments (Savage et al. 1999). This section reports the numerical calculations and simulations we conducted using Geochemist's Workbench 9.0 to investigate the chemical reactions in the analcite–calcite–acid (CO_2 acid or other acids) H_2O system, and proposes a genetic mechanism of the selective dissolution reaction.

6.1 Chemical reactions

The leaching reactions of analcite and calcite by CO_2 can be expressed by the following equations (Giles and Marshall 1986; Yuan et al. 2015a; Zhang et al. 2011):

$$\underset{\text{Analcite}}{NaAlSi_2O_6 \cdot H_2O} + CO_2(g) + 0.5H_2O = Na^+ + HCO_3^- + \underset{\text{Kaolinite}}{0.5Al_2Si_2O_5(OH)_4} + \underset{\text{Quartz}}{SiO_2}, \quad (1)$$

$$\underset{\text{K-feldspar}}{KAlSi_3O_8} + CO_2(g) + 1.5H_2O = \underset{\text{Kaolinite}}{0.5Al_2Si_2O_5(OH)_4} + \underset{\text{Quartz}}{2SiO_2} + K^+ + HCO_3^-, \quad (2)$$

$$\underset{\text{Calcite}}{CaCO_3} + CO_2(g) + H_2O = Ca^{2+} + 2HCO_3^-. \quad (3)$$

The log equilibrium constant of the above three reactions can be expressed as

$$\log K_1 = -\log f[CO_2(g)] - \log a[H_2O] + \log a[N^+] + \log a[HCO_3^-],$$

$$\log K_2 = \log a[K^+] + \log a[HCO_3^-] - \log f[CO_2(g)] - 1.5\log a[H_2O],$$

$$\log K_3 = \log a[Ca^{2+}] + 2\log a[HCO_3^-] - \log f[CO_2(g)] - \log a[H_2O].$$

Instead of CO_2, when other acids are used to leach analcite and calcite, the chemical reactions can be expressed by as follows:

$$NaAlSi_2O_6 \cdot H_2O + H^+ = 0.5H_2O + Na^+ + 0.5Al_2Si_2O_5(OH)_4 + SiO_2, \quad (4)$$

$$KAlSi_3O_8 + H^+ + 0.5H_2O = 0.5Al_2Si_2O_5(OH)_4 + 2SiO_2 + K^+, \quad (5)$$

$$CaCO_3 + H^+ = Ca^{2+} + HCO_3^-. \quad (6)$$

The log equilibrium constant of the above reactions can be expressed as

$$\log K_4 = -\log f[CO_2(g)] - \log a[H_2O] + \log a[N^+] + \log a[HCO_3^-],$$

$$\log K_5 = \log a[K^+] - \log a[H^+] - 0.5\log a[H_2O],$$

$$\log K_6 = \log a[Ca^{2+}] + 2\log a[HCO_3^-] - \log f[CO_2(g)] - \log a[H_2O].$$

The values of log equilibrium constant of the four reactions are shown in Fig. 11, where $\log K_1$ is higher than $\log K_2$ and $\log K_3$ is higher than $\log K_4$, indicating that the equilibrium constant of analcite leaching reactions are much higher than that of calcite leaching reactions.

6.2 Kinetic data

For kinetically controlled mineral dissolution and precipitation, the following simple rate law was applied (Yuan et al. 2015a):

$$r_m = k_m A_m (1 - Q/K), \quad (7)$$

where m is the mineral index, r_m is the reaction rate (mol/s, positive for dissolution and negative for precipitation), k_m is the rate constant (in mol/cm^2/s), A_m is the mineral's surface area (in cm^2), and Q and K are the activity product and equilibrium constants for the dissolution reaction, respectively. The temperature dependence of the reaction rate constant can be expressed reasonably well via the Arrhenius equation (Lasaga 1984; Steefel and Lasaga 1994). Because the rate constants for K-feldspar, calcite, and secondary minerals are generally reported at around 25 °C, it is reasonable to approximate the rate constant dependency as a function of temperature (Xu et al. 2005):

$$k = k_{25} \exp\left[\frac{-Ea}{R}\left(\frac{1}{T} - \frac{1}{298.15}\right)\right], \quad (8)$$

where Ea is the activation energy, k_{25} is the rate constant at 25 °C, R is the gas constant, and T is the absolute temperature.

Mineral dissolution and precipitation rates are a product of the kinetic rate constant and the reactive surface area described in Eq. (7). Parameters used for the kinetic rate expression of calcite and K-feldspar are provided in Table 1. Temperature-dependent kinetic rate constants were calculated using Eq. (8) and the precipitation of possible secondary minerals is represented utilizing the same kinetic expression as that used for dissolution. Nucleation was also considered in the current simulations for mineral precipitation. Scientific publications were referenced for kinetic parameters and the specific surface areas of calcite, analcite, quartz, and kaolinite with specific grain sizes.

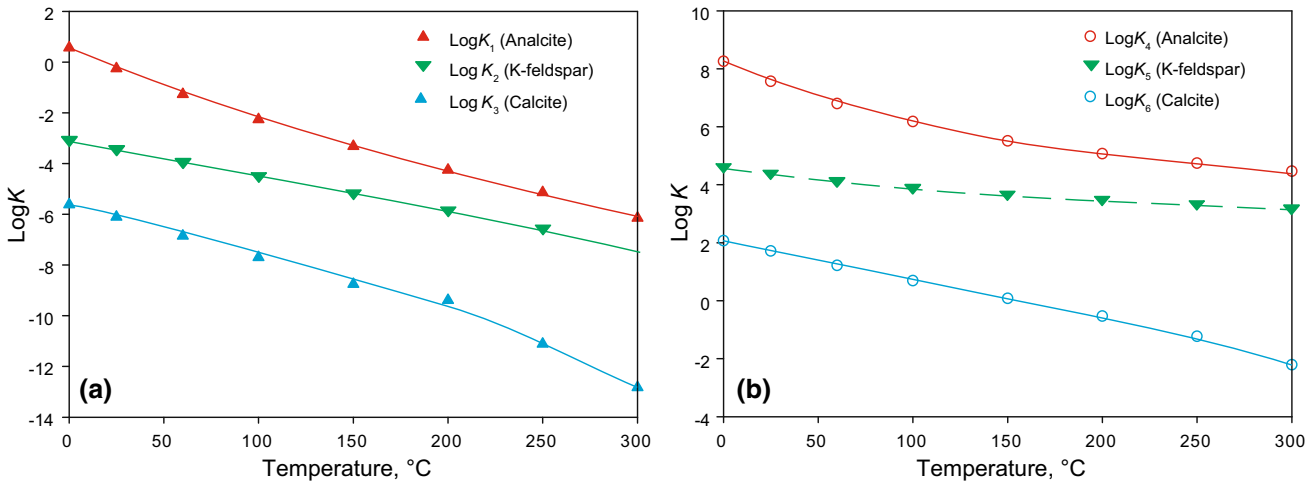

Fig. 11 Relations of temperature versus equilibrium constant in acid solution with analcite and calcite

Table 1 Kinetic data for different minerals used in numerical simulations

Minerals	K_m (25 °C), mol/cm^2/s	*Ea*, kJ/mol	K_m (80 °C), mol/cm^2/s	Specific surface area, cm^2/g	Nucleus, cm^2/cm^3	References
Calcite	1×10^{-9}	48.2	2.06×10^{-8}	2000	–	Pokrovsky et al. (2009); Sanz et al. (2011)
K-feldspar	1×10^{-17}	57.78	1.08×10^{-15}	1000	–	Kampman et al. (2009); Xu et al. (2005)
Analcite	–	–	3.16×10^{-14}	1800	–	Savage et al. (1999)
Quartz	1.26×10^{-18}	87.5	3.07×10^{-16}	1000	500	Harouiya and Oelkers (2004); Xu et al. (2005)
Kaolinite	1.26×10^{-17}	62.76	6.50×10^{-16}	10×10^4	500	Xu et al. (2005); Yang and Steefel (2008)

The evolution of surface area in natural geologic media is very complex and reported that specific surface areas vary based on mineral size and even literature reference. Specific surface areas of clean calcite grains measuring 125–250 and 25–53 μm by BET method were reported as 1700 and 2100 cm^2/g (Sanz et al. 2011), respectively. Also, the surface areas of calcite grains measuring 100–200 μm by BET method were reported as 662 cm^2/g according to Pokrovsky et al. (2005). The specific surface areas of clean K-feldspar and quartz grains measuring 50–100 μm by BET method were reported as 955 and 945 cm^2/g, respectively (Harouiya and Oelkers 2004), that for K-feldspar grains measuring 50–100 μm was 1400 cm^2/g (Alekseyev et al. 1997). Specific surface areas of clean analcite grains measuring 63–75, 45–63, and 32–45 μm by BET method were reported as 1700 and 2100 cm^2/g, respectively (Savage et al. 1999). The specific surface areas of clean K-feldspar and quartz grains measuring 50–100 μm were reported as 1030, 1450, and 830 cm^2/g, respectively, and the specific surface area of clean quartz grains measuring 50–100 μm was reported as 1000 cm^2/g (Harouiya and Oelkers 2004). For this study, the specific surface areas of 2000 cm^2/g for calcite and 1800 cm^2/g for analcite are used. Kaolinite has a much larger specific surface area, up to approximately 10×10^4 cm^2/g (Yang and Steefel 2008) (Table 1).

6.3 Pore water

Data of 40 pore water samples from sandstone reservoirs in the Xing'anling Group in the Suderte Oilfield show that the pore water is characterized by $NaHCO_3$-water. The salinity of pore water is very low, ranging from 1737 to 10,813 mg/L, with an average of 5689 mg/L. Primary ions consist mainly of Na^+, Cl^-, and HCO_3^- (Table 2). We employed one water sample with fairly average composition for numerical simulations.

6.4 Simulation results

6.4.1 Analcite–calcite–CO_2–H_2O system

Based on the diagenetic environment of the studied sandstones, 80 °C was employed in short-term (100 s) (Fig. 12) and long-term (1000 years) (Fig. 13) simulations, and 1.176 bar was set for partial pressure of CO_2 according to the equation $\log p_{CO_2} = -1.45 + 0.019T$ (Smith and Ehrenberg 1989). Our simulation results showed that the

Table 2 Composition of current pore water in the Xing'anling Group, Suderte Oilfield

	Salinity, mg/L	$Na^+ + K^+$, mg/L	Cl^-, mg/L	Ca^{2+}, mg/L	Mg^{2+}, mg/L	HCO_3^-, mg/L	SO_4^{2-}, mg/L
Maximum	10,813	6279	5021	114	50	3031	1575
Minimum	1737	436	272	1	1	0	66
Average	5689	1855	1356	29	17	1728	567
Sample no.	6548	4990	2184	24	10	1308	784

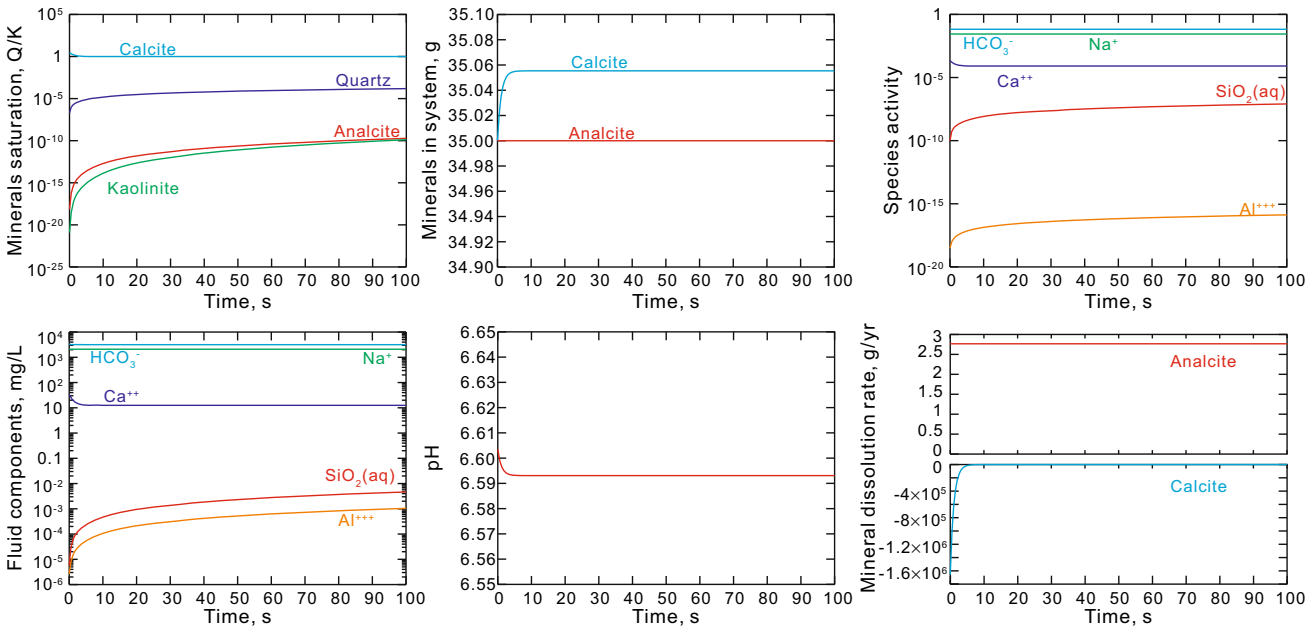

Fig. 12 Numerical simulation results of fluid-rock reactions in the calcite–analcite–CO_2–H_2O system for a short time (100 s)

chemical reaction processes at work in the reservoirs can be roughly divided into two stages.

Stage 1: Fast calcite precipitation—slow analcite dissolution (Fig. 12). At the beginning of the simulation, the mineral saturation index showed that pore water in the Xing'anling Formation was oversaturated with respect to calcite and undersaturated with respect to analcite, causing rapid calcite precipitation. Because the calcite reaction rate is high, this stage lasts a very short time (10 s). Only a little analcite can be dissolved in such a brief time, and the concentrations of Al^{3+} and SiO_2 (aq) in the fluids are low, so no precipitation of kaolinite or quartz occurs.

Stage 2: Slow calcite precipitation—slow analcite dissolution (Fig. 13). After stage 1, the mineral saturation index showed that pore water reached equilibrium with calcite while pore water was still undersaturated with analcite, leading to slow dissolution of analcite. As the concentrations of Al^{3+} and SiO_2 (aq) increased, the pore water became saturated with respect to kaolinite and quartz, leading to precipitation of secondary minerals. As the dissolution rate of analcite is very low, this stage could last a long time.

6.4.2 *Analcite–K-feldspar–CO_2–H_2O system*

Based on the diagenetic environment of the studied sandstones, 80 °C was used in the short-term (100 s) (Fig. 9) and long-term (1000 years) (Fig. 10) simulations, and 1.176 bar was set for partial pressure of CO_2 according to the equation $\log p_{CO_2} = -1.45 + 0.019T$ (Smith and Ehrenberg 1989). Simulation results showed that in the analcite–K-feldspar–CO_2–H_2O system, dissolution of large volumes of analcite occurred more easily than that of K-feldspar and at a much faster rate (Fig. 14). In effect, in the geochemical system consisting both of analcite and K-feldspar, extensive feldspar dissolution probably occurred later than analcite dissolution, which is consistent with the petrography texture of the few analcite remnants in the reservoirs in the Xing'anling Formation. As the concentrations of Al^{3+} and SiO_2 (aq) increased, the pore water became saturated with respect to kaolinite and quartz,

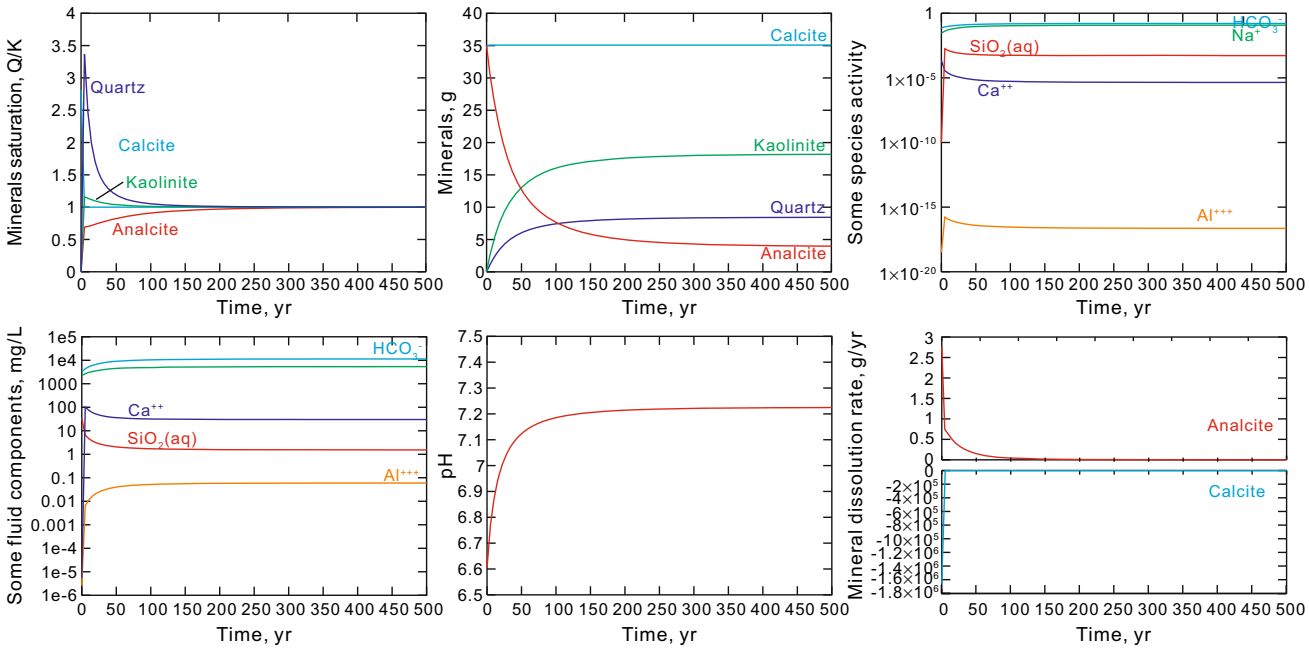

Fig. 13 Numerical simulation results of fluid-rock reactions in the calcite–analcite–CO_2–H_2O system for extended periods of time (500 years)

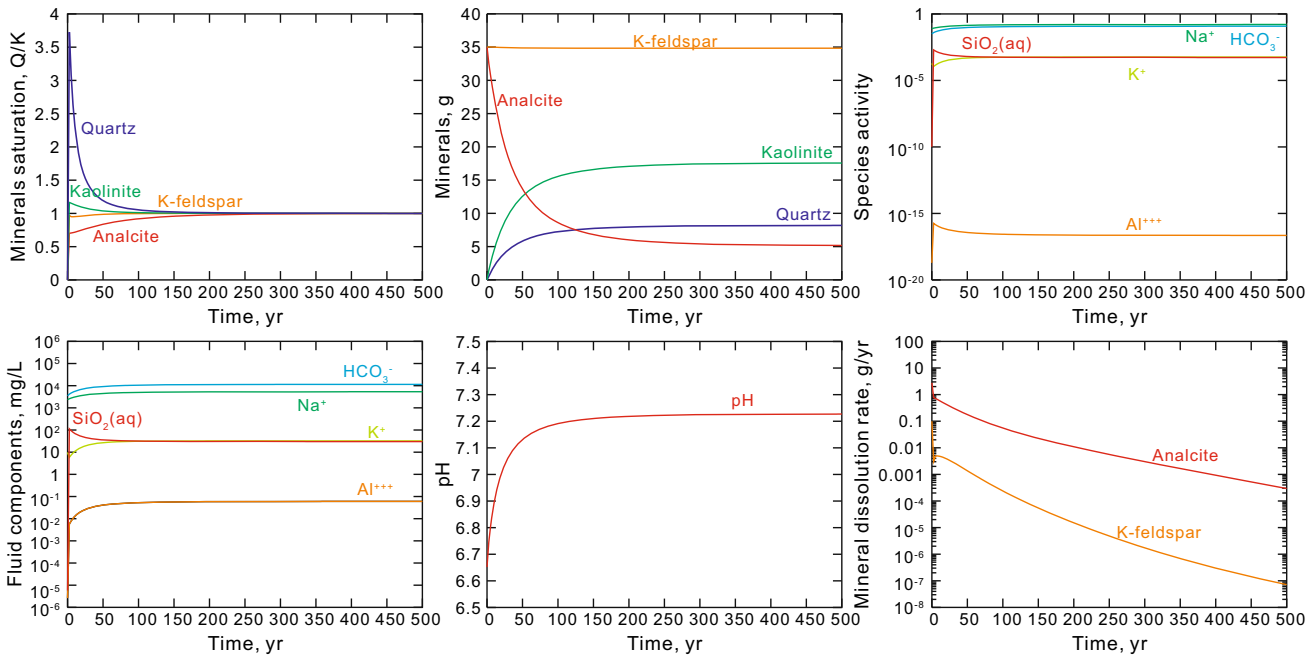

Fig. 14 Numerical simulation results of fluid-rock reactions in analcite–K-feldspar–CO_2–H_2O system for extended periods of time (500 years)

leading to precipitation of secondary minerals. Because the rate of analcite dissolution is very low, this stage lasts a long time.

A study by Yuan et al. (2015a) showed that feldspar dissolution occurs more easily than calcite dissolution in a geochemical system with both minerals. Constrained by pore water, equilibrium constants of different reactions, dissolution/precipitation rate, and saturation state of the pore water to minerals, analcite dissolution occurred more easily than calcite dissolution in the geochemical system with these two minerals, and analcite dissolution occurred more easily than feldspar dissolution in the geochemical

system with these two minerals. Thus, we concluded that in geochemical systems with analcite, K-feldspar, and calcite, the dissolution trend is analcite > K-feldspar > calcite. The selective dissolution of analcite and K-feldspar in the presence of calcite is an inevitable natural result, indicating that different early cements can develop different dissolution features during the mesodiagenetic period in the presence of acidic fluids. Understanding these processes substantially assists high-quality reservoir prediction.

7 Conclusions

The most notable conclusions and implications of this study can be summarized as follows.

1. The Xing'anling Group reservoirs with abundant volcanic materials in the Suderte Oilfield are low-permeability and ultra-low permeability reservoirs, texturally and compositionally immature. The reservoirs consist mainly of litharenite and feldspathic litharenite and have generally experienced compaction/early analcite cementation/early calcite cementation–feldspar dissolution/analcite dissolution/authigenic kaolinite precipitation/quartz cementation–late carbonate cementation.
2. The main early cements in the study area are calcite and analcite. In the mesodiagenetic stage, abundant analcite was selectively dissolved and calcite was left intact. The equilibrium constant of the calcite leaching reaction by acidic fluids is significantly lower than that of the analcite leaching reaction, indicating that in the analcite–calcite–CO_2–H_2O system, calcite is prone to reach the precipitation–dissolution equilibrium stage. Simulations with constraints of pore water and kinetics demonstrated that the pore water is supersaturated with respect to calcite, thus calcite cannot be dissolved, and that the water is undersaturated with respect to analcite, leading to extensive dissolution of analcite.
3. Selective dissolution of different early cements resulted in differing impacts on reservoir quality evolution. Reservoirs with abundant analcite exhibit favorable physical properties through burial dissolution of analcite cement at the mesodiagenetic stage, while reservoirs with abundant early calcite exhibit poor physical properties with no dissolution of calcite cement.

Acknowledgments This study is financially supported by the National Science and Technology Special Grant (No. 2011ZX05009-003), China Postdoctoral Science Fund (2015M580617), Shandong Postdoctoral Innovation Fund (201502028), and 2014 Innovation Project of China University of Petroleum (YCX2014002). We thank anonymous reviewers for their constructive comments.

References

Alekseyev VA, Medvedeva LS, Prisyagina NI, et al. Change in the dissolution rates of alkali feldspars as a result of secondary mineral precipitation and approach to equilibrium. Geochim Cosmochim Acta. 1997;61(6):1125–42.

Arvidson RS, Ertan IE, Amonette JE, et al. Variation in calcite dissolution rates: a fundamental problem? Geochim Cosmochim Acta. 2003;67(9):1623–34.

Bjørlykke K, Jahren J. Open or closed geochemical systems during diagenesis in sedimentary basins: constraints on mass transfer during diagenesis and the prediction of porosity in sandstone and carbonate reservoirs. AAPG Bull. 2012;96(12):2193–214.

Cao YC, Yuan GH, Wang YZ, et al. Genetic mechanisms of low permeability reservoirs of Qingshuihe Formation in Beisantai area, Junggar Basin. Acta Pet Sin. 2012;33(5):758–71 **(in Chinese)**.

Cao YC, Yuan GH, Li XY, et al. Characteristics and origin of abnormally high porosity zones in buried Paleogene clastic reservoirs in the Shengtuo area, Dongying Sag, East China. Pet Sci. 2014;11(3):346–62.

Chen CY, Gao YF, Wu HB, et al. Zircon U–Pb chronology and its stratigraphy implications for volcanic rocks from the Hailaer Basin. J Jilin Univ (Earth Sci Ed). 2015;45(S1):1503–19 **(in Chinese)**.

Cui JP, Ren ZL, Chen YL. Study on the relations between geothermal history and oil–gas generation in Beier depression of Hailaer Basin. Acta Sedimentol Sin. 2011;29(2):388–94 **(in Chinese)**.

Dutton SP, Loucks RG. Reprint of: diagenetic controls on evolution of porosity and permeability in lower Tertiary Wilcox sandstones from shallow to ultradeep (200–6700 m) burial, Gulf of Mexico Basin, USA. Mar Pet Geol. 2010;27(1):69–81.

Fu GM, Dong MC, Zhang ZS, et al. Formation process and distribution of laumontite in Yanchang 3 reservoir of Fuxian exploration area in north Shaanxi province and the controls of the high quality reservoirs. Earth Sci (J China Univ Geosci). 2010;35(1):107–14 **(in Chinese)**.

Giles MR. Mass transfer and problems of secondary porosity creation in deeply buried hydrocarbon reservoirs. Mar Pet Geol. 1987;4(3):188–204.

Giles MR, Marshall JD. Constraints on the development of secondary porosity in the subsurface: re-evaluation of processes. Mar Pet Geol. 1986;3(3):243–55.

Gluyas J, Coleman M. Material flux and porosity changes during sediment diagenesis. Nature. 1992;356(6364):52–4.

Han S, Yu H, Si C, et al. Corrosion of analcite in reservoir of Junggar Basin. Acta Pet Sin. 2007;28(3):51–4 **(in Chinese)**.

Harouiya N, Oelkers EH. An experimental study of the effect of aqueous fluoride on quartz and alkali-feldspar dissolution rates. Chem Geol. 2004;205(1–2):155–67.

Kampman N, Bickle M, Becker J, et al. Feldspar dissolution kinetics and Gibbs free energy dependence in a CO_2-enriched groundwater system, Green River, Utah. Earth Planet Sci Lett. 2009;284(3–4):473–88.

Lasaga AC. Chemical kinetics of water–rock interactions. J Geophy Res Solid Earth (1978–2012). 1984;89(B6):4009–25.

Lu ZX, Ye SJ, Yang X, et al. Quantification and timing of porosity evolution in tight sand gas reservoirs: an example from the Middle Jurassic Shaximiao Formation, western Sichuan, China. Pet Sci. 2015;12(2):207–17.

Macquaker JHS, Taylor KG, Keller M, et al. Compositional controls on early diagenetic pathways in fine-grained sedimentary rocks: implications for predicting unconventional reservoir attributes of mudstones. AAPG Bull. 2014;98(3):587–603.

Meng YL, Liang HT, Wei W, et al. Thermodynamic calculations of the laumontite dissolution and prediction of secondary porosity zones: a case study of horizon of Xujiaweizi fault depression. Acta Sedimentol Sin. 2013;31(3):509–15 **(in Chinese)**.

Meng YL, Zhu HD, Li XN, et al. Thermodynamic analyses of dolomite dissolution and prediction of the secondary porosity zones: a case study of tight tuffaceous dolomites of the second member, Permian Lucaogou Formation, Santanghu Basin, NW China. Pet Explor Dev. 2014;41(6):754–60.

Mousavi MA, Bryant SL. Geometric models of porosity reduction by ductile grain compaction and cementation. AAPG Bull. 2013;97(12):2129–48.

Pittman ED, Larese R. Compaction of lithic sands: experimental results and applications. AAPG Bull. 1991;75(8):1279–99.

Pokrovsky OS, Golubev SV, Schott J. Dissolution kinetics of calcite, dolomite and magnesite at 25 °C and 0 to 50 atm pCO_2. Chem Geol. 2005;217(3–4):239–55.

Pokrovsky OS, Golubev SV, Schott J, et al. Calcite, dolomite and magnesite dissolution kinetics in aqueous solutions at acid to circumneutral pH, 25 to 150 °C and 1 to 55 atm pCO2: new constraints on CO_2 sequestration in sedimentary basins. Chem Geol. 2009;265(1–2):20–32.

Qi SC. The diagenesis of the sandstone in Chang 8–10 Layer, Yanchang Formation, Longdong Region, late Triassic of Ordos Basin and the thermodynamic behavior of laumontite. Master Thesis, Chengdu University of Technology; 2013 **(in Chinese)**.

Sanz E, Ayora C, Carrera J. Calcite dissolution by mixing waters: geochemical modeling and flow-through experiments. Geol Acta. 2011;9(1):67–77.

Savage D, Rochelle C, Mihara M, et al. Dissolution of analcite under conditions of alkaline pH. Ninth annual VM Goldschmidt conference, August 22–27, 1999.

Schmidt V, McDonald DA. The role of secondary porosity in the course of sandstone diagenesis. SPEM Spec Publ. 1979;26:175–207.

Shen JN, Song T, Zhu J. Burial and subsidence history of Beier depression in Hailaer Basin. J Heilongjiang Inst Sci Technol. 2013;23(2):176–80 **(in Chinese)**.

Shou JF. Kinetics of Sandstone Diagenesis. Beijing: Petroleum Industry Press; 2005. p. 10–5 **(in Chinese)**.

Smith JT, Ehrenberg SN. Correlation of carbon dioxide abundance with temperature in clastic hydrocarbon reservoirs: relationship to inorganic chemical equilibrium. Mar Pet Geol. 1989;6(2):129–35.

Song T. The study of burial and subsidence history of Beier Depression in Hailar Basin. Ph.D. Dissertation. Daqing: Northeast Petroleum University; 2013 **(in Chinese)**.

Steefel CI, Lasaga AC. A coupled model for transport of multiple chemical species and kinetic precipitation/dissolution reactions with application to reactive flow in single phase hydrothermal systems. Am J Sci. 1994;294(5):529–92.

Sun YS, Liu XN, Zhang YQ, et al. Analcite cementation facies and forming mechanism of high-quality secondary clastic rock reservoirs in western China. J Palaeogeogr. 2014;16(4):517–26 **(in Chinese)**.

Surdam RC, Boese SW, Crossey LJ. The chemistry of secondary porosity: Part 2. Aspects of porosity modification. Paper in AAPG special volumes: clastic diagenesis; 1984. pp. 127–49.

Tang Z, Parnell J, Longstaffe FJ. Diagenesis and reservoir potential of Permian–Triassic fluvial/lacustrine sandstones in the southern Junggar Basin, northwestern China. AAPG Bull. 1997;81(11):1843–65.

Taylor TR, Giles MR, Hathon LA, et al. Sandstone diagenesis and reservoir quality prediction: models, myths, and reality. AAPG Bull. 2010;94(8):1093–132.

Turchyn AV, Depaolo DJ. Calcium isotope evidence for suppression of carbonate dissolution in carbonate-bearing organic-rich sediments. Geochim Cosmochim Acta. 2011;75(22):7081–98.

Wang JP, Fan TL, Wang HY, et al. Reservoir heterogeneity characteristics in the framework of multi-grade base level cycle of the oil layers of Tongbomiao and Nantun Formations in the Suderte Oil Field. Earth Sci Front. 2012;19(2):141–50 **(in Chinese)**.

Xi KL, Cao YC, Wang YZ, et al. Factors influencing physical property evolution in sandstone mechanical compaction: the evidence from diagenetic simulation experiments. Pet Sci. 2015;12(3):391–405.

Xiao YY, Fan TL, Wang HY. Characteristics and diagenesis of the volcaniclastic rock reservoirs from the Nantun Formation within the Suderte structural zone in the Buir depression. Sedim Geol Tethyan Geol. 2011;31(2):91–8 **(in Chinese)**.

Xiu HW. Diagenesis research and reservoir evaluation in Quan3 and Quan4 Members of northern Songliao Basin. Ph.D. Dissertation, Northeast Petroleum University; 2008 **(in Chinese)**.

Xu T, Apps JA, Pruess K. Mineral sequestration of carbon dioxide in a sandstone–shale system. Chem Geol. 2005;217(3–4):295–318.

Xu ZY, Zhang XY, Wu SH, et al. Genesis of the low-permeability reservoir bed of upper Triassic Xujiahe Formation in Xinchang gas field, western Sichuan Depression. Pet Sci. 2008;5(3):230–7.

Yang L, Steefel CI. Kaolinite dissolution and precipitation kinetics at 22 °C and pH 4. Geochim Cosmochim Acta. 2008;72(1):99–116.

Yu BS, Lai XY. Carbonic acid system of groundwater and the solubility of calcite during diagenesis. Acta Sedimentol Sin. 2006;24(5):627–35 **(in Chinese)**.

Yuan GH, Cao YC, Yang T, et al. Porosity enhancement potential through mineral dissolution by organic acids in the diagenetic process of clastic reservoir. Earth Sci Front. 2013;20(5):207–19 **(in Chinese)**.

Yuan GH, Cao YC, Gluyas J, et al. Feldspar dissolution, authigenic clays, and quartz cements in open and closed sandstone geochemical systems during diagenesis: typical examples from two sags in Bohai Bay Basin, East China. AAPG Bull. 2015a;99(11):2121–54.

Yuan GH, Cao YC, Jia ZZ, et al. Selective dissolution of feldspars in the presence of carbonates: the way to generate secondary pores in buried sandstones by organic CO_2. Mar Pet Geol. 2015b;60:105–19.

Yuan GH, Gluyas J, Cao YC, et al. Diagenesis and reservoir quality evolution of the Eocene sandstones in the northern Dongying Sag, Bohai Bay Basin, East China. Mar Pet Geol. 2015c;62:77–89.

Zhang XH, Huang SJ, Lan YF, et al. Thermodynamic calculation of laumontite dissolution and its geologic significance. Lithol Reserv. 2011;23(2):64–9 **(in Chinese)**.

Zhang Q, Zhu XM, Steel RJ, et al. Variation and mechanisms of clastic reservoir quality in the Paleogene Shahejie Formation of the Dongying Sag, Bohai Bay Basin, China. Pet Sci. 2014;11(2):200–10.

Zhao GQ. Study of petrological characteristics and thermodynamic mechanism of secondary pores in deep reservoirs, Songliao Basin. Ph.D. Dissertation, China University of Geosciences (Beijing); 2005 **(in Chinese)**.

Zhao L, Gao FH, Zhang YL, et al. Zircon U–Pb chronology and its geological implications of Mesozoic volcanic rocks from the Hailaer Basin. Acta Pet Sin. 2013;29(3):864–74 **(in Chinese)**.

Zhong D, Zhu X, Zhang Z, et al. Origin of secondary porosity of Paleogene sandstone in the Dongying Sag. Pet Explor Dev. 2003;30(6):51–3 **(in Chinese)**.

Zhu GH. Formation of lomonitic sand bodies with secondary porosity and their relationship with hydrocarbons. Acta Pet Sin. 1985;6(1):1–8 **(in Chinese)**.

Zhu XM, Wang YG, Zhong DK, et al. Pore types and secondary pore evolution of Paleogene reservoirs in the Jiyang Sag. Acta Geol Sin. 2007;81(2):197–204 **(in Chinese)**.

Zhu XM, Zhu SF, Xian BZ, et al. Reservoir differences and formation mechanisms in the Ke-Bai overthrust belt, northwestern margin of the Junggar Basin, China. Pet Sci. 2010;7(1):40–8.

Zhu SF, Zhu XM, Wang XL, et al. Zeolite diagenesis and its control on petroleum reservoir quality of Permian in northwestern margin of Junggar Basin. Sci China Earth Sci. 2011;41(11): 1602–12 **(in Chinese)**.

Zhu SF, Zhu XM, Wang XL, et al. Zeolite diagenesis and its control on petroleum reservoir quality of Permian in northwestern margin of Junggar Basin, China. Sci China Earth Sci. 2012;55(3):386–96.